Atmos. Chem. Phys. Discuss., 14, 13271–13300, 2014
www.atmos-chem-phys-discuss.net/14/13271/2014/
doi:10.5194/acpd-14-13271-2014

Atmospheric Chemistry and Physics Discussions

Optical, microphysical and compositional properties of the Eyjafjallajökull volcanic ash

A. Rocha-Lima[1], J. V. Martins[1,2], L. A. Remer[1], N. A. Krotkov[2], M. H. Tabacniks[3], Y. Ben-Ami[4], and P. Artaxo[3]

[1]University of Maryland, Baltimore County, Baltimore, MD, USA
[2]NASA Goddard Space Flight Center, Greenbelt, MD, USA
[3]Institute of Physics, University of Sao Paulo, Sao Paulo, Brazil
[4]Weizmann Institute of Science, Rehovot, Israel

Received: 28 February 2014 – Accepted: 28 April 2014 – Published: 22 May 2014

Correspondence to: A. Rocha-Lima (limadri1@umbc.edu)

Published by Copernicus Publications on behalf of the European Geosciences Union.

Abstract

Microphysical, optical, and compositional properties of the volcanic ash from the April–May (2010) Eyjafjallajökull volcanic eruption are presented. Samples of the volcanic ash were taken on the ground in the vicinity of the volcano. The material was sieved, re-suspended, and collected on filters, separating particle sizes into coarse and fine modes. The spectral mass absorption efficiency α_{abs} [$m^2\,g^{-1}$] was determined for coarse and fine particles in the wavelength range from 300 to 2500 nm. Size distribution of particles on filters was obtained using a semi-automatic software to analyze images obtained by Scanning Electron Microscopy (SEM). The grain density of the volcanic ash was determined as 2.16(13) g cm^{-3} by measuring the variation of air volume in a system with volcanic ash and air under compression. Using Mie–Lorenz and T-matrix theories, the imaginary part of the refractive index was derived. Results show the spectral imaginary refractive index ranging from 0.001 to 0.005. Fine and coarse particles were analyzed by X-Ray fluorescence for elemental composition. Fine and coarse mode particles exhibit distinct compositional and optical differences.

1 Introduction

After almost 200 years from its last eruption, the Eyjafjallajökull volcano on the southern edge of Iceland initiated seismic activity in April 2010. Although the eruption is considered to be of small to moderate size, the volcanic ash injected into the atmosphere spread over much of Europe due to fine particle fragmentation during magma-ice interaction and weather conditions that facilitated the rapid transport of the plume toward European airspace. The spread caused an unprecedented interruption of the aircraft traffic in Europe with important economic and social impacts (Gudmundsson et al., 2010; Langmann et al., 2012).

Volcanic eruptions are an important source of aerosols to the atmosphere. While volcano eruptions can directly affect the weather in the near regions, large volcanic

eruptions can also produce global effects (Robock, 2000). During an eruption, volcanoes can inject gases and solid particles directly into the upper troposphere and lower stratosphere. Gases, mainly in the form of water vapor, sulfur, and carbon dioxide, can have a short and long term effect on climate respectively (Morse and Mackenzie, 1990). Some of the sulfur gas emitted by the volcano oxidizes downstream to become sulfate particles. These sulfate particles should not be confused with the actual solid material (volcanic ash) injected directly by the eruption.

In addition to the environment effects, previous volcanic eruptions have shown to be hazardous for aviation (Pieri et al., 2002; Casadevall, 1994). Volcanic ash can melt and coat engine components, reducing efficiency and restricting ventilation of the engine. Hard and sharp fragments of the volcanic ash are highly abrasive and can scratch airplane components (Neal et al., 2004).

During the last Eyjafjallajökull volcanic eruption, the scientific community combined information from ground, aircraft (Schumann et al., 2011; Newman et al., 2012; Rauthe-Schöch et al., 2012) and remote sensing (Ansmann et al., 2010; Gasteiger et al., 2011) to evaluate the actual conditions and to recommend air traffic restrictions.

Mass concentration is the usual quantity required to judge safety limits of the airspace.The retrieval of the mass concentration by optical techniques including in situ and remote sensing requires some assumptions about the microphysical properties of the volcanic ash (Newman et al., 2012). The mass absorption, scattering and extinction efficiencies [$m^2\,g^{-1}$] are the main quantities connecting the optical properties and the bulk mass of the aerosol particles. In general, size distribution, shape, and refractive index are assumed known in order to derive the ash mass concentration in the atmosphere. In addition, the spectral dependence of the refractive index, particularly the imaginary part, is usually unknown for most aerosol particles including volcanic ash. The uncertainty in the refractive index and the assumptions of spherical shape and internal mixtures are the main sources of error in the retrieval of optical depths (Ilyinskaya et al., 2011). It is also important to evaluate how particle shape should be taken into account when retrieving the refractive index (Krotkov et al., 1998; Yi et al., 2011).

The knowledge of microphysical and optical properties of volcanic ash aerosols are essential for the remote sensing of aerosols and for atmospheric correction models that are needed for many types of retrievals and analyses. In this study, the spectral optical properties of the Eyjafjallajökull volcanic ash sample were derived over a broad spectral range, from ultra-violet (UV) to near infrared (NIR) wavelengths. The sample of the Eyjafjallajökull volcanic ash collected on the ground was initially sieved, resuspended and re-collected on filters. Several analytical techniques were used to characterize the ash samples. Scanning electron microscopy (SEM) data were used to get the shape and size distribution. X-Ray Fluorescence (XRF) was used to obtain the chemical composition of the volcanic ash. The density of the grain was measured independently using a Densimetry method, and Reflectance analyses were used to derive the mass absorption efficiency.

The imaginary part of the refractive index was calculated through an iterative inversion process. This calculation was obtained by combining the *Empirical power law method* and the *Size distribution method*, as will be described in the following sections.

Both Mie–Lorenz theory and the T-Matrix code (Mishchenko et al., 1996) were applied for the determination of the refractive index with the assumption of spherical and spheroid particle shape respectively.

2 Experimental methods and analyses

2.1 Volcanic ash resuspension and filter collection

The volcanic ash sample studied in this research was collected on the ground about 35 km from the volcano Eyjafjallajökull at the village of Vik (63.42° N 10.01° W) on 8 May 2010, 4 weeks after the first volcanic eruption. The sample was shoveled into a small bag from the ground.

At the Laboratory of Aerosols, Clouds, and Optics (LACO) at the University of Maryland, Baltimore County (UMBC), the material was initially sieved to retain particles

smaller than 45 µm. Particles larger than 45 µm were discarded and not analyzed due to their short residence time in the atmosphere. Figure 1 shows, respectively, (A) the original sample, as it was collected on the ground, (B) discarded fraction with particles larger than 45 µm and (C) the fraction below 45 µm retained to be re-suspended.

We found that approximately 1/3 of the mass of the original material collected on the ground was formed by particles smaller than 45 µm.

Sieved particles (C) smaller than 45 µm were submitted to a re-suspension procedure in a Fluidized Bed Aerosol Generator (FBAG) – TSI Model 3400A where they were disaggregated down to submicron sizes and carried out by a flow of dry air (Fig. 2). A cyclone and an impactor, at the exit nozzle of the FBAG were used to remove particles larger than 10 µm. Nuclepore® filters with pores of 5 µm (coarse filter) and 0.4 µm (fine filter) in diameter were used to collect the coarse and fine modes respectively. The Nuclepore filters work like an impactor, and therefore pores with 0.4 µm diameter have collection efficiency close to 100 % for all particle sizes. Filters with 5 µm pores have cutoff sizes around 1.5 µm (Buzzard et al., 1981).

A high precision analytical microbalance was used to determine the particle mass collected on the filters. The filters were weighed before and after the deposition of the resuspended particles for the determination of the concentration σ in [g m^{-2}], of the mass deposited per unit of area on the surface of each filter.

2.2 SEM analysis and size distribution

Scanning Electron Microscopy (SEM) analysis provided information of shape and size distribution of the particles. A semi-automatic procedure using *ImageJ* software (Abràmoff et al., 2004), was used to determine the top view cross section area of each particle. From this area, the diameter of an equivalent circular area was derived.

The *ImageJ* software is not able to distinguish particles that are too close to each other or overlapped, particles partially on the border of the figure, and particles that don't contrast well with the background of the image. In these cases a second evaluation was performed manually using the software *PhotoImpact X3* to take into account these particles separately.

Figure 3 shows SEM images of a fine filter. Black circles on the images are the filter pores while the particles are shown in white. The second image shows an example of analyzed particles by the *ImageJ* software.

Figure 4 shows the particle's number, surface area, and volume distribution for the fine (red) and coarse (blue) fraction based on an analysis of about 3000 particles. Most of the particles collected on the fine filter have diameter below 2 µm while coarse filter contains particles that overlap the fine filter but also extend to 11 µm of diameter.

2.3 Grain density of the volcanic ash

The density ρ of the volcanic ash was measured using an instrument similar to the gas pycnometer (Chang, 1988). The volume V_{ash} of a sample was obtained by measuring the variation of the volume (ΔV) required to double the pressure of the vessel, as illustrated in Fig. 5. We repeat this procedure with and without the volcanic ash particle inside the vessel. The equations in the drawing were solved to produce the volume V_{ash} and to determine the density as $\rho = M_{ash}/V_{ash}$, where M_{ash} is the mass of the analyzed sample.

The measured volcanic ash density was 2.16(13) g cm^{-3}. This value is smaller than what is usually used in the literature for ash samples from the Eyjafjallajökull volcano, which is 2.6 g cm^{-3} (Gasteiger et al., 2011; Bukowiecki et al., 2011) or 2.4 g cm^{-3} (Gudmundsson et al., 2010).

2.4 Spectral light absorption via reflectance measurements

The spectral light absorption of the volcanic ash particles was investigated by measuring the reflectance of the Nuclepore® filters as a function of the volcanic ash collected mass. A broad band light source was used to shine light on these filters. The reflected light from the loaded filters was analyzed comparatively to blank filters reflectivity. Two

spectrometers with different broad band illuminators were used: Avantes – AvaSpec 2048 – from ultra-violet (UV) starting from 300 nm to near infrared wavelenths (NIR) up to 1100 nm and FieldSpec Pro – Analytical Spectral Devices from 350 to 2500 nm.

Figure 6 shows the spectral reflectance for the Eyjafjallajökull volcanic ash collected on several filters with different mass loadings. We can see from these results that most of the attenuation occurs for short wavelengths and we will assume that the total attenuation is due mainly to absorption. The reasoning behind this assumption is based on two properties of our experimental setup: (1) Light scattered forward by the particles will most likely hit the white surface of the filter underneath and scatter backward on its path back to the spectrometer; (2) Reflectance of aerosol particles on filters was measured at different viewing angles (from 10 to 45° from nadir) and found to be constant within 5 %. These measurements demonstrated that the angular effects of phase function and/or filter BRDF (Bidirectional Reflectance Distribution Function) are not significant in this range.

According to Martins et al. (2009), when particles are attached to the filters, a correction of the Lambert–Beer law is needed to describe the absorption of light by these particles. This correction was derived using an empirical power coefficient $b = 1.218$ and it is described in this paper as the *Empirical Power Law Method* where the relationship between σ and the mass absorption efficiency α_{abs} is given by Eq. (1).

$$\sigma = \frac{G}{2\alpha_{\text{abs}}}[-\ln(I/I_0)]^b + c \tag{1}$$

The mass absorption efficiency α_{abs} in [$\text{m}^2\,\text{g}^{-1}$] can be obtained by the relationship between the collected aerosol mass per unit of area on the surface of the filter σ[$\text{g}\,\text{m}^{-2}$] and the logarithm of the reflectance fraction (I/I_0) for each wavelength. Here I/I_0 is the ratio of the reflectance of a filter with ash deposited on it and one clean filter. The geometrical factor G described in Martins et al. (2009) was determined to equal one for a large range of geometries including the one used in this work. The parameter c is

a constant to take into account a possible offset in the mass of the filters, for instance due to an error in blank subtraction.

Figure 7 shows examples of power law fittings for 350 nm and 550 nm using the Empirical Power Law Method for fine filters with different loaded masses. This fit was performed for each wavelength every 1 nm from 300 nm to 2500 nm, allowing us to obtain the spectral dependence of $\alpha_{\text{abs}} = G/(2a)$.

Figure 8 shows the resulting mass absorption efficiency obtained from the *Empirical Power Law Method* applied for each measured wavelength, as exemplified in Fig. 7. The results show enhanced UV absorption features for fine particles. This is in agreement with the fact that large particles, in the range considered, lower the absorption efficiency due to incomplete light penetration into the particle (Moosmuller et al., 2011).

Another independent method to obtain the mass absorption efficiency is based on the particles' size distribution, referred to as *Size distribution method*. The mass absorption (or scattering, or extinction) efficiency of the aerosols (α_i in [$\text{m}^2\,\text{g}^{-1}$], where the index i indicates either absorption, scattering or extinction) can be written in terms of the particle number size distribution ($n(r)$ in [particles m^{-2}]), geometrical cross section ($A(r)$ [m^2]), volume of each particle ($v(r)$ [m^3]) and grain density (ρ [$\text{g}\,\text{m}^{-3}$]) of the material by

$$\alpha_i = \frac{\int_0^\infty n(r)Q_i(x,m)A(r)\mathrm{d}r}{\int_0^\infty n(r)\rho v(r)\mathrm{d}r} \tag{2}$$

Q_i is the efficiency coefficient representing the weighting factor for the probability of interaction of light with particles. Q_i depends on the particle size parameter $x = 2\pi r/\lambda$, and on the complex refractive index of the particle material $m = n - ik$.

Volcanic ash particles have a diversity of shapes, as can be seen in Fig. 3. The relation between shape of the particles and their absorption properties is not fully understood for complicated shape distributions. Here we used the comparison between spherical particles and spheroids to assess the sensitivity of our retrieved imaginary refractive index to particle shape. Q_{abs} was calculated using (1) Mie–Lorenz Theory,

with the assumption of spherical particles, and (2) T-matrix, with the assumption of spheroids.

2.5 Refractive Index derivation

The imaginary part of the refractive index Im(m) for coarse and fine particles of the Eyjafjallajökull volcanic ash was obtained by an iterative process that minimizes the difference between α_{abs} derived from Eq. (1) and α_{abs} obtained from Eq. (2) for each wavelength.

We performed this minimization for different values of Re(m) within a trusted interval to obtain Im(m). This way we could estimate the influence of Re(m) on the minimization procedure. The mean value found for Re(m) equals 1.68. For this sample, we have observed that a change in Re(m) from 1.58 to 1.78 produces a 0.0005 change in Im(m).

Figure 9 shows the results obtained for Im(m) with Re(m) kept fixed at its mean value. High imaginary indices are observed for wavelengths bellow 500 nm with a strong increase in the UV region. A minimum of absorption is observed at $\lambda = 875$ nm for fine particles, and at $\lambda = 700$ nm for the coarse ones. For shorter wavelengths, Im(m) for the fine particles is higher than the coarse ones with an inversion for longer wavelengths. The crossover is at about $\lambda = 550$ nm.

The uncertainties on the retrieval of Im(m) were estimated considering the main sources of errors in our retrieval: the real part of the refractive index and the density of the material. These uncertainties are shown as error bars in Fig. 9. Errors from the size distribution, mainly due to the miscounting of particles and to statistical errors, were found to be smaller (< 3 %) compared to the error of the real part of the refractive index and density measurements.

In the literature, the refractive index of the Eyjafjallajökull volcanic ash was reported as Re(m) = 1.58(2) and Im(m) in the range 0.002 – 0.015i (at 550 nm), derived using the Particle Soot Absorption Photometer inversion method (Weinzierl et al., 2012; Petzold et al., 2009, 2011). In Schumann et al. (2011) the Eyjafjallajökull volcanic ash

plume was studied assuming absorbing particles with refractive index $1.59 + 0.004i$ and non-absorbing particles with refractive index $1.59 + 0i$ at 636 nm. Differences on the refractive index between fine and coarse particles due to chemical composition variations were also discussed by Newman et al. (2012); this study adopted $1.52 + 0.0015i$ for coarse mode and $1.43 + 0.00i$ for fine mode, specified across all UV-visible wavelengths. These results from literature are partially in agreement with those we found in this work. Comparatively to other volcanic ashes, our imaginary refractive index in UV has the same order of magnitude of previous laboratory measurements for Mount Spurr volcano (Krotkov et al., 1999). However, our results have smaller imaginary refractive index than Mount St. Helens and Fuego ashes measured in the 80's (Patterson et al., 1981, 1983).

The T-matrix method was also applied assuming randomly oriented nonspherical particles using the extended-precision code. A modified gamma function was fitted to the measured size distribution of the particles showed in Fig. 4. Using the SEM images, the median of the aspect ratio distribution was obtained calculating the axial ratio of each particle. The most probable value for the aspect ratio was found to be $f = 1.5$ for both fine and coarse distributions and this value was used in the T-matrix code. Implications of this assumption were evaluated in Sect. 3 where other values of $f = 1.8$ and 3.0 were also used for T-matrix calculations.

Figure 10 overlaps the imaginary refractive indices derived using Mie Theory and T-matrix methods for fine particles. The high agreement indicates, at least in the range considered, that a change of aspect ratio from $f = 1$ (spherical case) to 1.5 (oblate spheroid) does not produce significant variation in the imaginary refractive index. The agreement between Mie and T-Matrix for fine particles was also observed by Krotkov et al. (1999).

In the coarse mode, the combination of large particles ($d > 3\,\mu$m) and smaller wavelengths (below 1 µm) generated large size parameters for which the T-matrix code produced convergence errors that did not allow the final calculations of the absorption efficiencies.

2.6 Compositional analysis by X-Ray Fluorescence

Energy Dispersive X-ray Fluorescence analysis (EDXRF) of the fine and coarse particles was used to investigate the dependence of the refractive indices with chemical composition. X-ray Fluorescence analyses of twelve fine filters and four coarse filters were performed at the Atmospheric Physics Laboratory at University of Sao Paulo on an Epsilon 5 PanAnalytical EDXRF spectrometer.

Figure 11 shows the average concentration fraction (for fine and coarse particles) relative to the total mass collected on the filters. Si, Al and Fe are the three major elements that together represent up to 35 % of the total aerosol mass.

The ratios between the fine and coarse average concentrations calculated based only on the mass detected by EDXRF (from Na to Pb) presented in Fig. 12 show the variation between fine and coarse elemental concentrations. The results show a tendency for low atomic number elements to dominate in the fine particles while higher atomic number elements dominate in the coarse particles. Lower levels of Na, Mg, Al for coarse particles might be explained by a possible size-dependent self absorption enhancement not taken into account during the EDXRF analysis. The higher ratio obtained for sulfur is in agreement with the presence of the sulfate particles (around 150 nm) that are produced by sulfuric acid drops and they are expected to be concentrated mostly in the fine mode (Weinzierl et al., 2012).

Samples with fine and coarse particles of the volcanic ash were submitted to thermal optical carbon analysis, but no significant amount of carbon was found.

3 Discussion

We found that the mass absorption efficiencies for fine and coarse modes are different. These differences in the mass absorption efficiency between the modes should not be attributed only to differences in the refractive index, but also to the size distributions of the particles (Moosmuller et al., 2011).

The retrieved imaginary refractive index is slightly different for fine and coarse particles. The EDXRF analysis also show different composition for fine and coarse mode particles, which relates to the difference in refractive index. This finding is corroborated by other studies of volcanic ash from the same volcanic eruption that showed differences of compositions between the modes (Schumann et al., 2011; Newman et al., 2012). Further studies and discussions on this dependence of particles' composition with their size in minerals can be found in Kandler et al. (2009).

It is also important to discuss the assumptions of the particles' shapes for the retrieval of the refractive index. The retrieval initially considered all particles as spheres, allowing for the retrieval of the imaginary part of the refractive index using Mie theory. The sensitivity of the retrieval of the imaginary part of the aerosol refractive index to non-spherical particles was studied using the T-matrix code. This study was done for the fine mode only. A constant aspect ratio $f = 1.5$ was selected initially as a representative value for fine mode aerosols based on the median of the measured aspect ratio distribution measured from the scanning electron microscopy pictures of the particles (Fig. 13a). In order to evaluate the effect of the non-sphericity of the particles, Fig. 13b shows the retrieval of the imaginary part of the refractive index considering higher aspect ratios $f = 1.8$ and $f = 3.0$ for this analysis. We found that $f = 1.8$ is the highest value of f that we could run T-matrix without convergence problems for the entire range of wavelengths we studied in this work. By considering $f = 3.0$, we are certainly overestimating the effects of shape on the retrieval, although this value of f limited us to obtain results for wavelengths only above 1100 nm. As can be seen in Fig. 13b, the effects of assumptions on the shape of the particles are not negligible. But even the most conservative analysis considering $f = 3.0$ produced results that are within the uncertainties previously estimated for the imaginary part of the refractive index.

4 Conclusions

The results obtained show differences in the optical properties between fine and coarse fraction of the analyzed volcanic ash. These differences were observed in the spectral mass absorption efficiency and in the imaginary part of the refractive index. From 300 to 550 nm, the imaginary part of the refractive index for fine particles varies between 0.0015 to 0.0055i, while for coarse particles the variation in the same wavelength interval is from 0.0015 to 0.003. From 550 nm to 2500 nm, the imaginary refractive index for coarse and fine modes varies from 0.001 to 0.002. The method is suitable to the derivation of the imaginary part of the refractive index and the real part should be constrained within a trusted limit. The range of the trusted limit of the real part together with the uncertainty of the density of the material are the main sources of error in the derivation of the imaginary part. Assuming spherical or spheroid particle shapes in calculations of the mass absorption efficiency both yield similar imaginary refractive indices for fine particles.

EDXRF analysis shows that fine and coarse particles have compatible composition for most of the elements. Notable differences are observed for Ca and Fe (the forth and the fifth more abundant element), the ratio of their concentrations seems to indicate slightly higher concentrations of Ca and Fe in the coarse particles. The double concentration of sulfur in the fine particles, even though in small amount, is in agreement with the expected higher concentration of fine sulfur particles produced by sulfuric acid drops. Further studies are needed to explain the relationship between the differences of composition and optical properties observed between fine and coarse particles.

Acknowledgements. We acknowledge funding support from the NASA Atmospheric Composition Program (Investigation of Aerosol Spectral Absorption Properties from UV to NIR, grant number NNX07AT47G) and from the JCET/UMBC 2013–14 Graduate Fellowship. We thank the scientific and technical support of the LACO team at UMBC (especially Dominik Cieslak and Steven Buczkowski), and the LFA team at University of Sao Paulo (Ana Loureiro and Andrea Arana). We also thank Ulrich Schumann from DRL and Haraldur Olafsson for providing samples collected in Iceland and for providing information about the collection process. Y. Ben-Ami thanks the support of NASA Postdoctoral Program at the Goddard Space Flight Center.

References

Abràmoff, M. D., Magalhães, P. J., and Ram, S. J.: Image processing with ImageJ, Biophotonics International, 11, 36–42, 2004. 13275

Ansmann, A., Tesche, M., Groß, S., Freudenthaler, V., Seifert, P., Hiebsch, A., Schmidt, J., Wandinger, U., Mattis, I., Muller, D., and Wiegner, M.: The 16 April 2010 major volcanic ash plume over central Europe: EARLINET lidar and AERONET photometer observations at Leipzig and Munich, Germany, Geophys. Res. Lett., 37, L13810, doi:10.1029/2010GL043809, 2010. 13273

Bukowiecki, N., Zieger, P., Weingartner, E., Jurányi, Z., Gysel, M., Neininger, B., Schneider, B., Hueglin, C., Ulrich, A., Wichser, A., Henne, S., Brunner, D., Kaegi, R., Schwikowski, M., Tobler, L., Wienhold, F. G., Engel, I., Buchmann, B., Peter, T., and Baltensperger, U.: Ground-based and airborne in-situ measurements of the Eyjafjallajökull volcanic aerosol plume in Switzerland in spring 2010, Atmos. Chem. Phys., 11, 10011–10030, doi:10.5194/acp-11-10011-2011, 2011. 13276

Buzzard, G. H. and Parker, R. D.: A two stage particle fractinator using large pore nuclepore surfaces, US Environmental Protection Agency, Environmental Sciences Research Laboratory, Research Triangle Park, N.C., USA, 1981. 13275

Casadevall, T. J.: Volcanic Ash and Aviation Safety, in: Proceedings of the First International Symposium on Volcanic Ash and Aviation Safety, US Geological Survey USGS Bulletin 2047, 1–6, 1994. 13273

Chang, C. S.: Measuring density and porosity of grain Kernels using a gas Pycnometer, Cereal Chem., 65, 13–15, 1988. 13276

Gasteiger, J., Groß, S., Freudenthaler, V., and Wiegner, M.: Volcanic ash from Iceland over Munich: mass concentration retrieved from ground-based remote sensing measurements, Atmos. Chem. Phys., 11, 2209–2223, doi:10.5194/acp-11-2209-2011, 2011. 13273, 13276

Gudmundsson, M. T., Pedersen, R., Vogfjörd, K., Thorbjarnardóttir, B., Jakobsdóttir, S., and Roberts, M. J.: Eruptions of Eyjafjallajökull volcano, Iceland, EOS T. Am. Geophys. Un., 91, 190–191, doi:10.1029/2010EO210002, 2010. 13272, 13276

Ilyinskaya, E., Tsanev, V. I., Martin, R. S., Oppenheimer, C., Le Blond, J., Sawyer, G. M., and Gudmundsson, M. T.: Near-source observations of aerosol size distributions in the eruptive plumes from Eyjafjallajökull volcano, March–April 2010, Atmos. Environ., 45, 3210–3216, doi:10.1016/j.atmosenv.2011.03.017, 2011. 13273

Kandler, K., Schütz, L., Deutscher, C., Ebert, M., Hofmann, H., Jäckel, S., Jaenicke, R., Knippertz, P., Lieke, K., Massling, A., Petzold, A., Schladitz, A., Weinzierl, B., Wiedensohler, A., Zorn, S., and Weinbruch, S.: Size distribution, mass concentration, chemical and mineralogical composition and derived optical parameters of the boundary layer aerosol at Tinfou, Morocco, during SAMUM 2006, Tellus B, 61, 32–50, 2009. 13282

Krotkov, N. A., Bhartia, P. K., Herman, J. R., Fioletov, V., and Kerr, J.: Satellite estimation of spectral surface UV irradiance in the presence of tropospheric aerosols: 1. Cloud-free case, J. Geophys. Res., 103, 8779–8793, doi:10.1029/98JD00233, 1998. 13273

Krotkov, N. A., Flittner, D. E., Krueger, A. J., Kostinski, A., Riley, C., Rose, W., and Torres, O.: Effect of particle non-sphericity on satellite monitoring of drifting volcanic ash clouds, J. Quant. Spectrosc. Ra., 63, 613–630, doi:10.1016/S0022-4073(99)00041-2, 1999. 13280

Langmann, B., Folch, A., Hensch, M., and Matthias, V.: Volcanic ash over Europe during the eruption of Eyjafjallajökull on Iceland, April–May 2010, Atmos. Environ., 48, 1–8, doi:10.1016/j.atmosenv.2011.03.054, 2012. 13272

Martins, J. V., Artaxo, P., Kaufman, Y. J., Castanho, A. D., and Remer, L.: Spectral absorption properties of aerosol particles from 350–2500 nm, Geophys. Res. Lett., 36, L13810, doi:10.1029/2009GL037435, 2009. 13277

Mishchenko, M. I., Travis, L. D., and Mackowski, D. W.: T-matrix computations of light scattering by nonspherical particles: a review, J. Quant. Spectrosc. Ra., 55, 535–575, doi:10.1016/0022-4073(96)00002-7, 1996. 13274

Moosmüller, H., Chakrabarty, R. K., Ehlers, K. M., and Arnott, W. P.: Absorption Ångström coefficient, brown carbon, and aerosols: basic concepts, bulk matter, and spherical particles, Atmos. Chem. Phys., 11, 1217–1225, doi:10.5194/acp-11-1217-2011, 2011. 13278, 13281

Morse, J. W. and Mackenzie, F. T.: Geochemistry of Sedimentary Carbonates, Elsevier, the Netherlands, 1990. 13273

Neal, C. A., Casadevall, T. J., Miller, T. P., Hendley II, J. W., and Stauffer, P. H.: Volcanic Ash: Danger to Aircraft in the North Pacific, US Geological Survey Fact Sheet 030-97, available at: http://volcanoes.usgs.gov/hazards/tephra/ashandaircraft.php (last access: February 2014), 2004. 13273

Newman, S. M., Clarisse, L., Hurtmans, D., Marenco, F., Johnson, B., Turnbull, K., Havemann, S., Baran, A. J., O'Sullivan, D., and Haywood, J.: A case of study of observations of volcanic ash from the Eyjafjallajökull eruption: 2. Airbone and satellite radiative measurements, J. Geophys. Res., 117, D00U13, doi:10.1029/2011JD016780, 2012. 13273, 13280, 13282

Patterson, E. M.: Optical properties of the crustal aerosol: Relation to chemical and physical characteristics, J. Geophys. Res., 86, 3236–3246, doi:10.1029/JC086iC04p03236, 1981. 13280

Patterson, E. M., Pollard, C. O., and Galindo, I.: Optical propertiesof the ash from El Chichon volcano, Geophys. Res. Lett., 10, 317–320, doi:10.1029/GL010i004p00317, 1983. 13280

Petzold, A., Rasp, K., Weinzierl, B., Esselborn, M., Hamburger, T., Dörnbrack, A., Kandler, K., Schütz, L., Knippertz, P., Fiebig, M., and Virkkula, A.: Saharan dust absorption and refractive index from aircraft-based observations during SAMUM 2006, Tellus B, 61, 118–130, doi:10.1111/j.1600-0889.2008.00383.x, 2009. 13279

Petzold, A., Veira, A., Mund, S., Esselborn, M., Kiemle, C., Weinzierl, B., Hamburger, T., Ehret, G., Lieke, K., and Kandler, K.: Mixing of mineral dust with urban pollution aerosol over Dakar (Senegal): impact on dust physico-chemical and radiative properties, Tellus B, 63, 619–634, doi:10.1111/j.1600-0889.2011.00547.x, 2011. 13279

Pieri, D., Ma, C., Simpson, J., Hufford, G., Grindle, T., and Grove, C.: Analysis of in-situ airborne volcanic ash from the February 2000 eruption of Hekla volcano, Iceland, Geophys. Res. Lett., 29, 1772, doi:10.1029/2001GL013688, 2002. 13273

Rauthe-Schöch, A., Weigelt, A., Hermann, M., Martinsson, B. G., Baker, A. K., Heue, K.-P., Brenninkmeijer, C. A. M., Zahn, A., Scharffe, D., Eckhardt, S., Stohl, A., and van Velthoven, P. F. J.: CARIBIC aircraft measurements of Eyjafjallajökull volcanic clouds in April/May 2010, Atmos. Chem. Phys., 12, 879–902, doi:10.5194/acp-12-879-2012, 2012. 13273

Robock, A.: Volcanic eruptions and climate, Rev. Geophys., 38, 191–219, doi:10.1029/1998RG000054, 2000. 13273

Schumann, U., Weinzierl, B., Reitebuch, O., Schlager, H., Minikin, A., Forster, C., Baumann, R., Sailer, T., Graf, K., Mannstein, H., Voigt, C., Rahm, S., Simmet, R., Scheibe, M., Lichtenstern, M., Stock, P., Rüba, H., Schäuble, D., Tafferner, A., Rautenhaus, M., Gerz, T., Ziereis, H., Krautstrunk, M., Mallaun, C., Gayet, J.-F., Lieke, K., Kandler, K., Ebert, M., Weinbruch, S., Stohl, A., Gasteiger, J., Groß, S., Freudenthaler, V., Wiegner, M., Ansmann, A.,

Tesche, M., Olafsson, H., and Sturm, K.: Airborne observations of the Eyjafjalla volcano ash cloud over Europe during air space closure in April and May 2010, Atmos. Chem. Phys., 11, 2245–2279, doi:10.5194/acp-11-2245-2011, 2011. 13273, 13279, 13282

Seinfeld, J. H. and Pandis, S. N.: Atmospheric Chemistry and Physics: from Air Pollution to Climate Change, Wiley-Interscience, USA, 1998. 13291

Weinzierl, B., Sauer, D., Minikin, A., Reitebuch, O., Dahlkötter, F., Mayer, B., Emde, C., Tegen, I., Gasteiger, J., Petzold, A., Veira, A., Kueppers, U., and Schumann, U.: On the visibility of airborne volcanic ash and mineral dust from the pilot's perspective in flight, Phys. Chem. Earth, 45–46, 87–102, doi:10.1016/j.pce.2012.04.003, 2012. 13279, 13281

Yi, B., Hsu, C. N., Yang, P., and Tsay, S.-H.: Radiative transfer simulation of dust-like aerosols: uncertainties from particle shape and refractive index, J. Aerosol Sci., 42, 631–644, doi:10.1016/j.jaerosci.2011.06.008, 2011. 13273

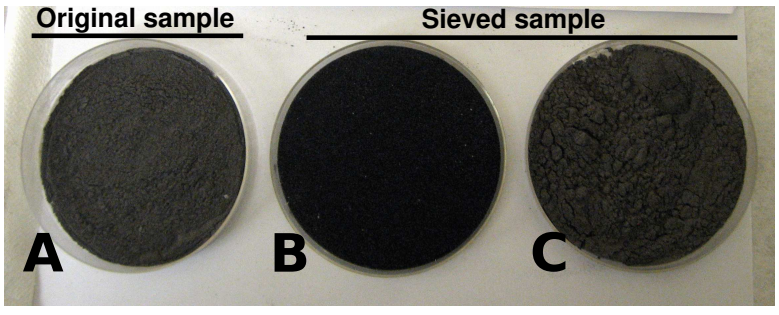

Figure 1. Samples of Volcanic ash from April 2010 Eyjafjallajökull eruption. **(A)** Original sample collected from the ground. **(B)** Fraction removed by sieving process (particles larger than 45 µm). **(C)** Fraction re-suspended for analysis (particles smaller than 45 µm).

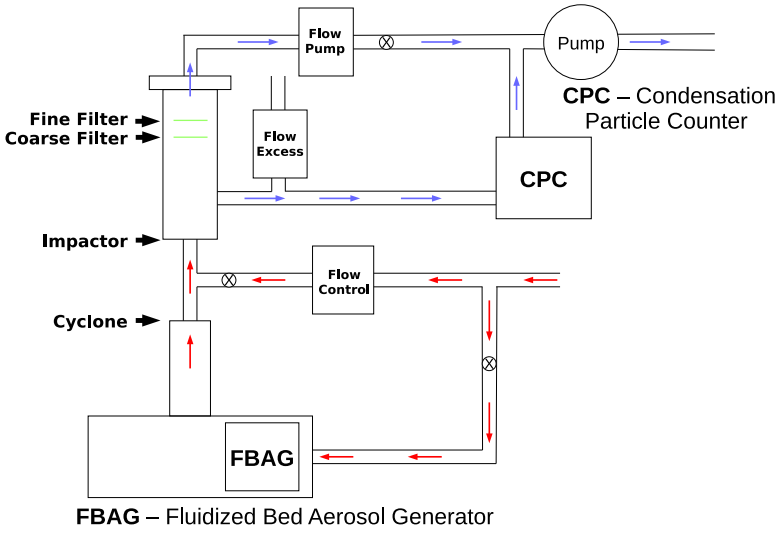

Figure 2. Sketch of experimental setup showing the Fluidized Bed Aerosol Generator (FBAG) at the bottom with air flow lines for aerosol re-suspension.

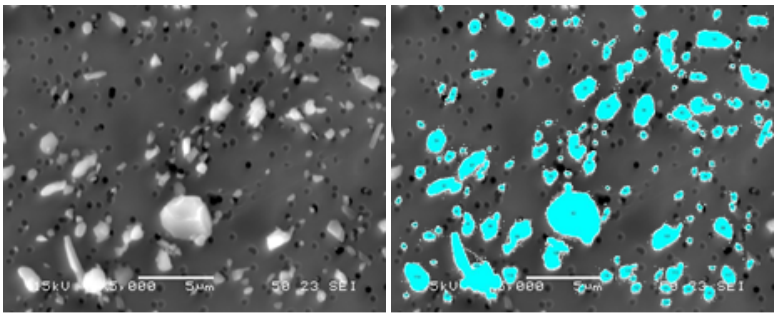

Figure 3. SEM images of the Eyjafjallajökull volcanic ash collected from the ground, resuspended and re-collected on filters. **(A)** Volcanic ash particles collected on a fine filter −0.4 µm pores. **(B)** Analyzed particles using *Image J* software showing top view cross sectional area of each particle.

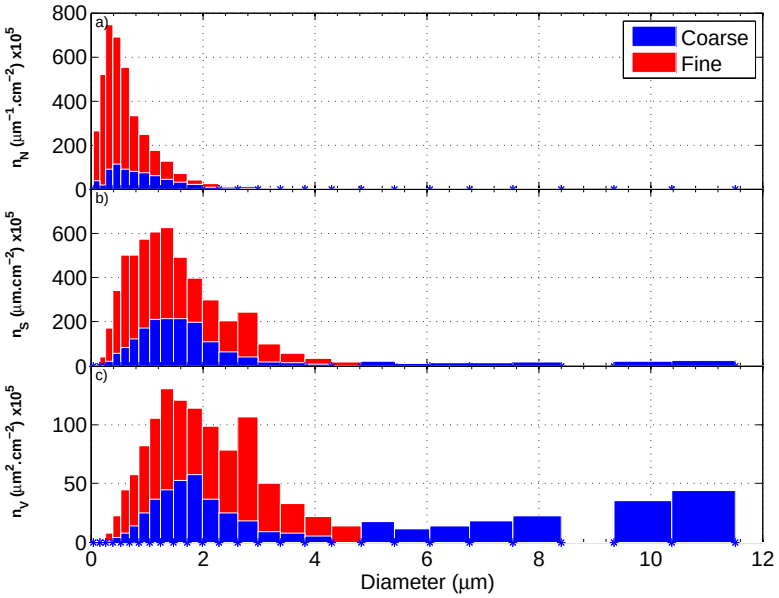

Figure 4. Particle's number, surface area, and volume distribution vs. particle diameter (per cm^2 of filters) obtained by analysis of SEM images for a fine and a coarse filter of the Eyjafjallajökull volcanic ash. Distributions are normalized by the width of the bins to show the area bellow the curve proportional to the number concentration, as presented in Seinfeld and Pandis (1998).

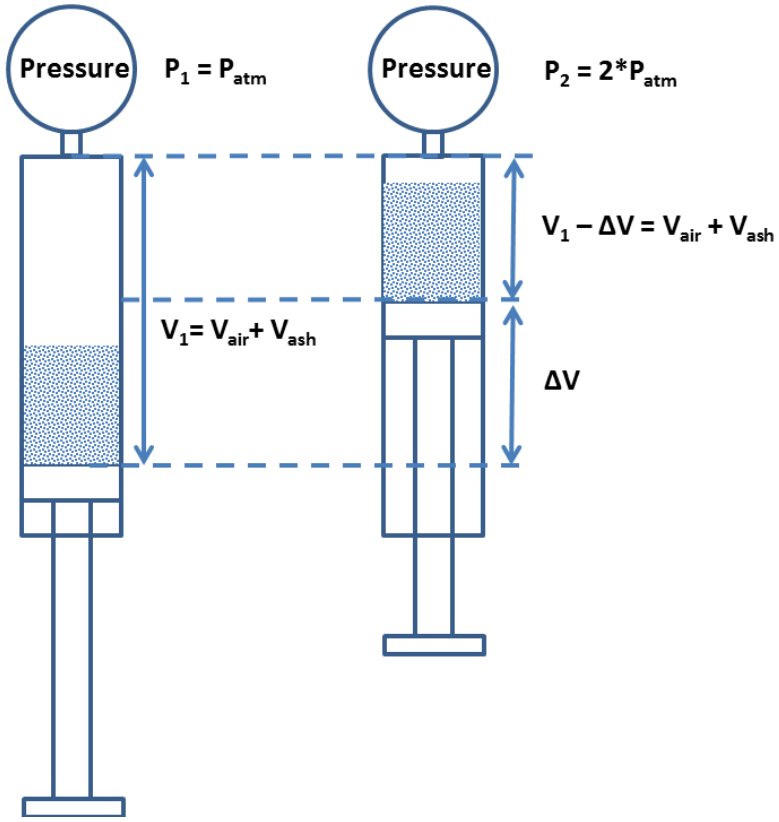

Figure 5. Schematic drawing of the experimental procedure for determination of the density of the volcanic ash.

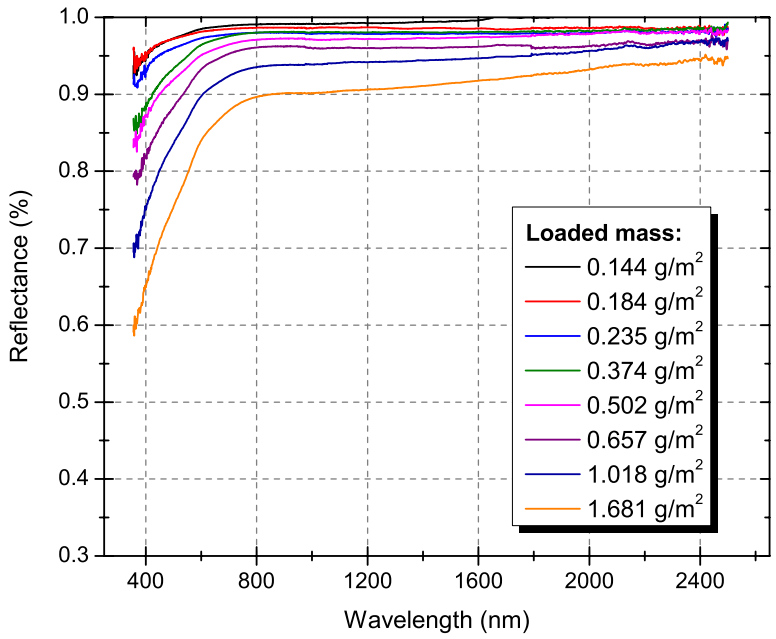

Figure 6. Spectral reflectance of the volcanic ash Eyjafjallajökull for fine filters according to the loaded mass per unit area σ of each filter in [g m^{-2}].

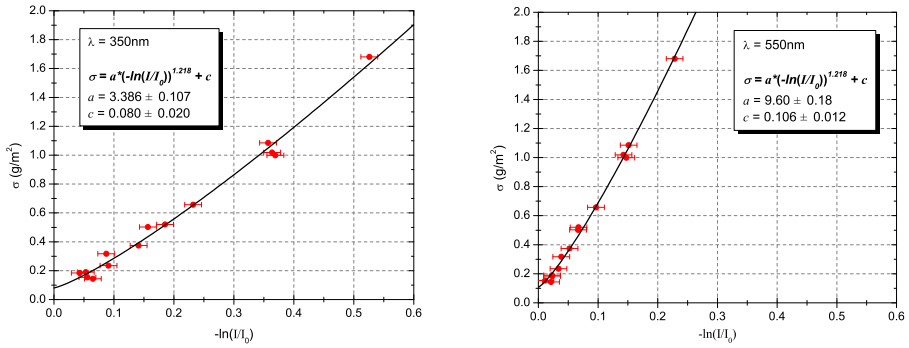

Figure 7. Power law fitting using b = 1.218 and a and c as free parameters. The shown examples are for fine particles of the Eyjafjallajökull volcanic ash for two wavelengths: 350 nm and 550 nm.

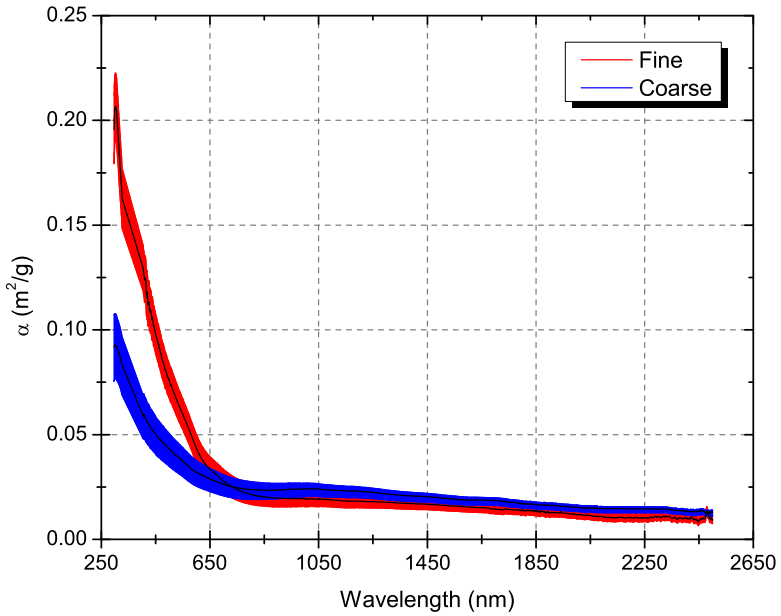

Figure 8. Spectral mass absorption efficiency (α_{abs}) for coarse and fine particles of the Eyjafjallajökull volcanic ash collected on filters. Uncertainties of the measurements are shown as error bands.

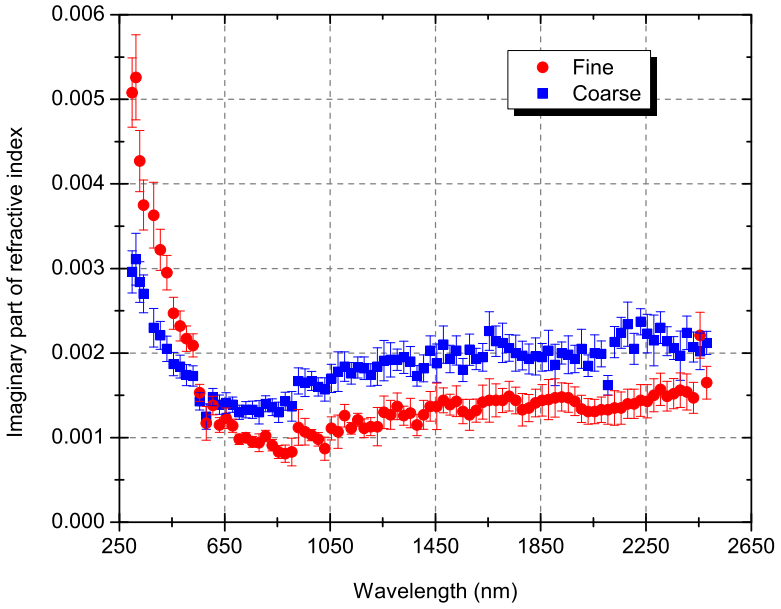

Figure 9. Imaginary refractive index for coarse and fine particles using Mie Theory with $n = 1.68$ and density $\rho = 2.16\,\mathrm{g\,cm^{-3}}$.

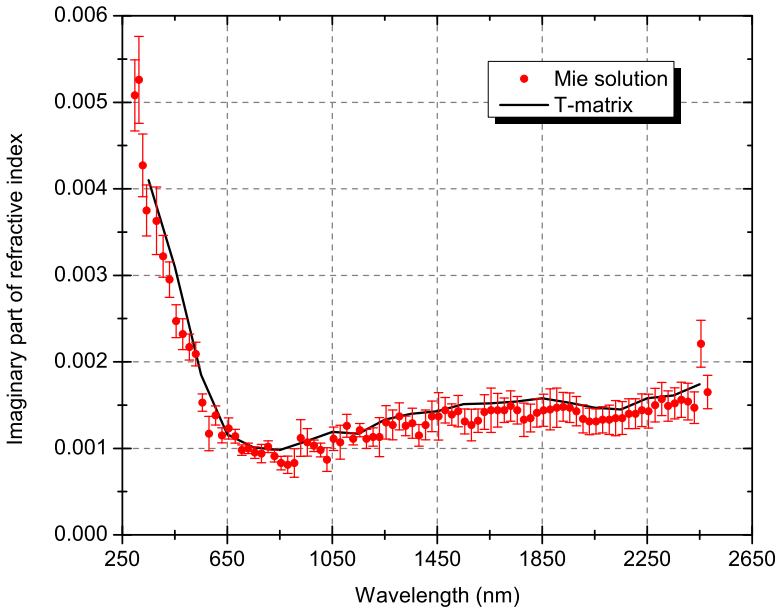

Figure 10. Imaginary refractive index calculated for fine particles by Mie Theory and T-Matrix (for an aspect ratio of 1.5).

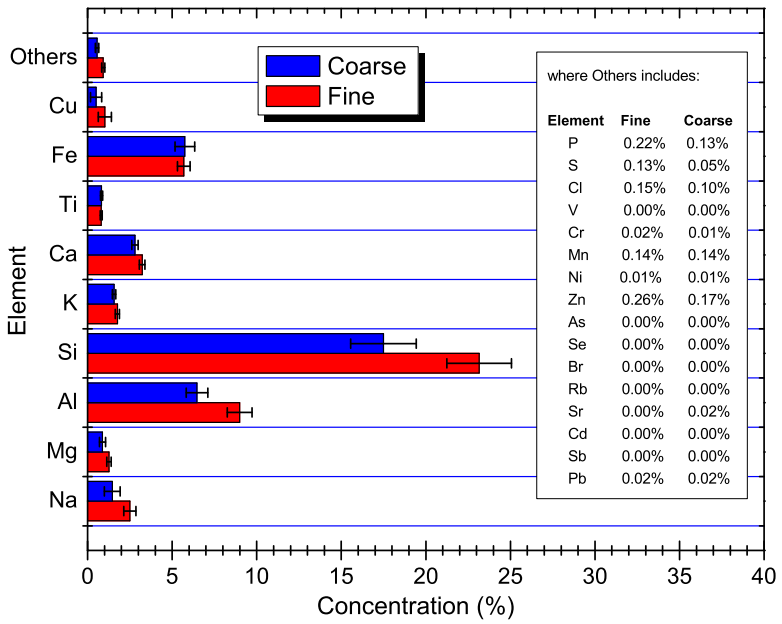

Figure 11. Fraction of the mass of each element in relation to the total collected mass.

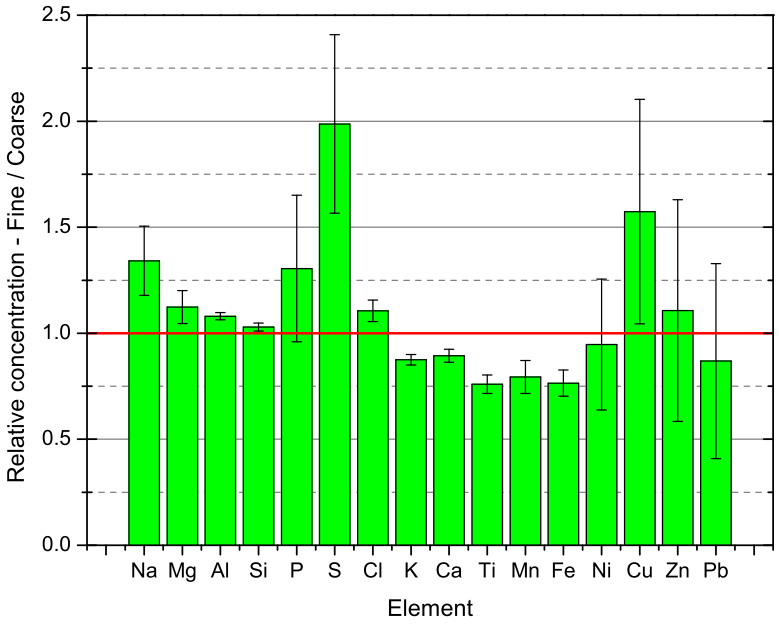

Figure 12. Relative mass concentration between fine and coarse modes.

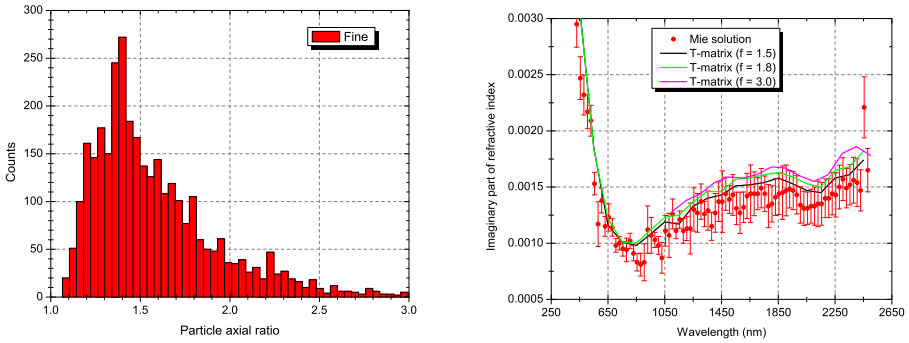

Figure 13. (A) Particles' shape distribution for the fine mode of the volcanic ash and **(B)** analysis of the imaginary part of the refractive index considering different aspect ratios f for the T-matrix calculations of spheroidal particles. For $f = 3$, the refractive index was retrieved only for wavelengths above 1100 nm due to convergence issues of the T-matrix code for shorter wavelengths.